Chapter 1

2-D field tests

INTRODUCTION AND SUMMARY

The tomography method described in the preceding chapter is suited for a particular class of problem. Generating raypaths and picking reflectors requires the dataset to be relatively clean with strong, fairly continuous reflectors. Formulating the tomography in tau is universally advantageous, but shows the most significant improvement over conventional techniques when velocity is not monotonically increasing. Finally, this method assumes that velocity generally follows structural dip, making a steering filter an effective regularization operator.

The North Sea dataset provided to SEP by TotalFinaElf. meets all of these criteria. The data is very clean (Figure 1.1) with strong reflectors that are generally continuous. The data contains a chalk layer which causes a velocity inversion below it. The initial velocity model (Figure 1.2) was created by IFP using the S.M.A.R.T[1] method (Jacobs et al., 1992; Ehinger and Lailly, 1995). The velocity structure shows typical North Sea behavior with velocity following structural layers.

The dataset is 3-D marine acquired using four cables with geophones every 25 meters. In this chapter I will be dealing with a 2-D subset of the 3-D dataset. The line was chosen to

[1]Sequential Migration-Aided Reflection Tomography - KIM (Kinematic Inversion Methods), IFP consortium

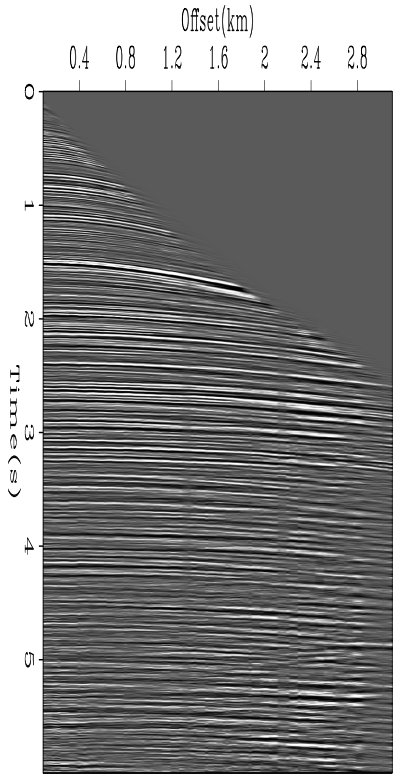

Figure 1.1: A preprocessed shot gather from the L7D dataset. 2d-elf-shot [ER]

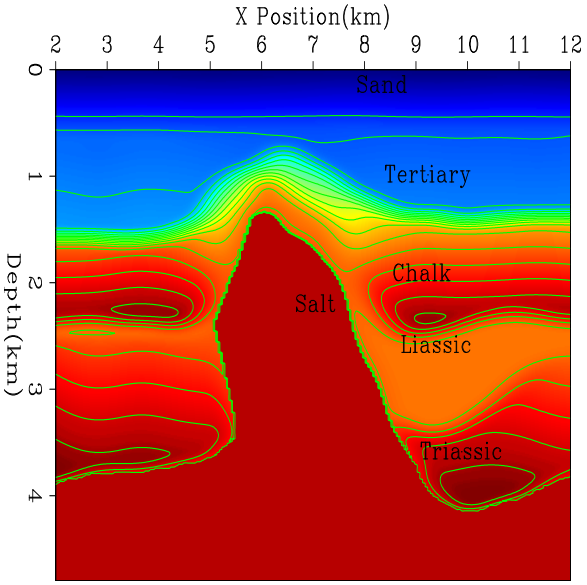

Figure 1.2: The initial velocity model for the 2-D line. Overlaid are the general geologic units in the area. Note how the velocity follows structural dip and that velocity decrease below the chalk layer in the Liassic. 2d-vel0 [CR]

coincide with a 2-D synthetic dataset (Prucha et al., 1998; Malcotti and Biondi, 1998). The subset was created by forming partial stacking and then applying Azimuth Moveout (AMO) (Biondi et al., 1998) to the CMP gathers.

I will begin this chapter by showing the migration and moveout errors with the initial velocity. Next, I will show how I built the steering filter operator and some of the issues involved in dealing with the complex salt structure. I will then move onto applying the tomography technique to the dataset.

INITIAL ERRORS

Figure 1.3 is result of migrating the data with the velocity of Figure 1.2. The strong chalk reflection ('D') is low frequency and focusing problems make its amplitude suspiciously space-variant. The salt is generally poorly defined. The salt top reflection ('B') is discontinuous. The bottom of the salt ('C') is poorly imaged. The most interesting problem is along the salt edge ('A') where we see little reflector continuity below 2.8 km. If we look at the CRP gathers (Figure 1.4) we see significant moveout and focusing problems.

Using the initial migrated image I chose 11 reflectors to perform tomography with (Figure 1.5). To constrain the upper portion of the model I chose the water bottom reflection and two reflectors above the salt. I picked the salt top and salt bottom and three reflectors on both sides of the salt body.

I performed moveout analysis using equation (**??**). I selected the semblance at each reflector, Figure 1.6, and found a smooth curve using fitting goals (**??**). The top two reflectors have have almost no moveout errors and the third reflector very little. The remaining reflectors all have some residual moveout errors that tomography can attempt to resolve.

BUILDING THE STEERING FILTERS

For constructing the steering filters I used the same methodology as described in Chapter **??**. I first calculated the dip along the nine non-salt reflectors and then interpolated to the entire

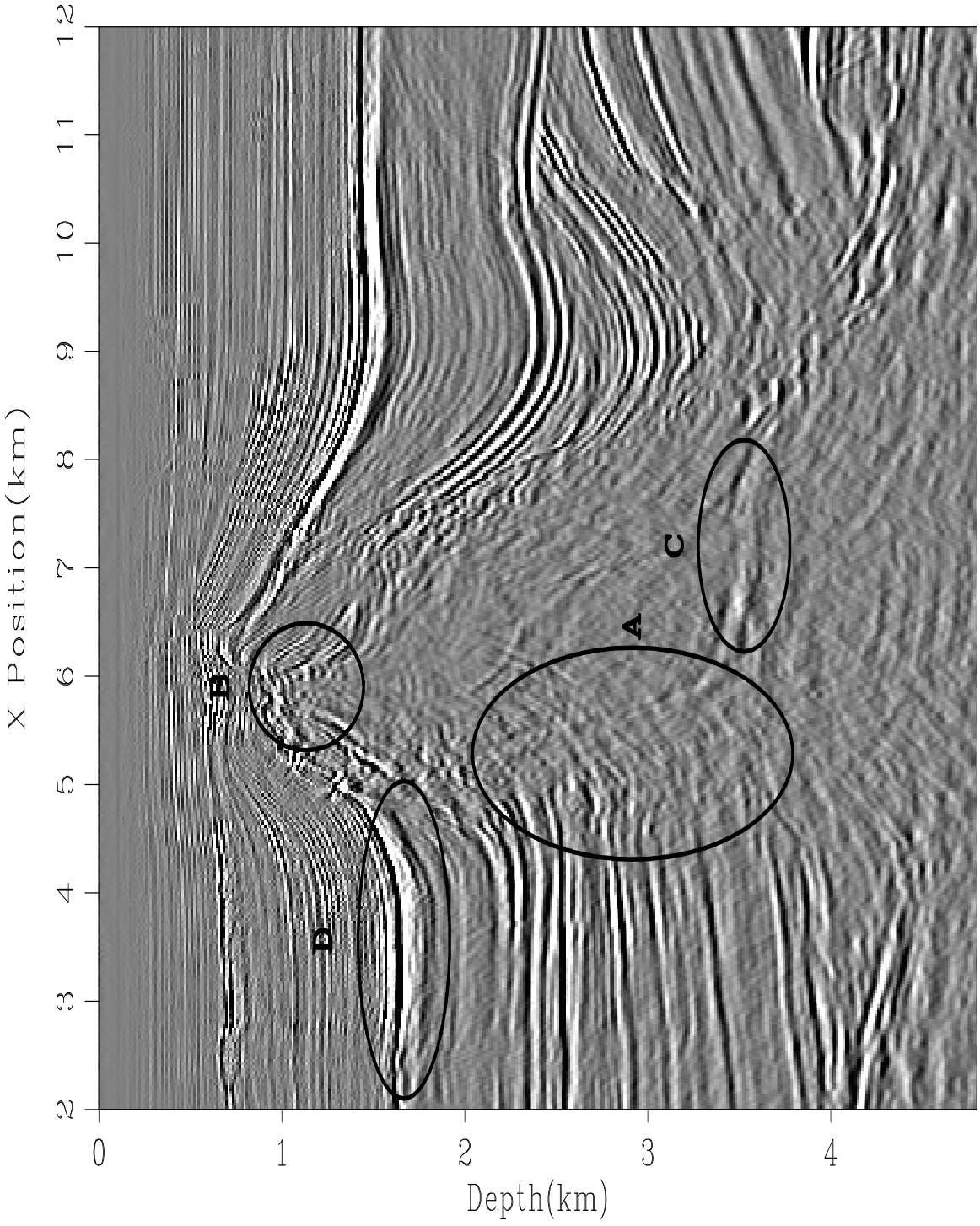

Figure 1.3: Migration result using the velocity from Figure 1.2. Migrations problems can be seen at locations A-D. 2d-elf-mig0 [CR]

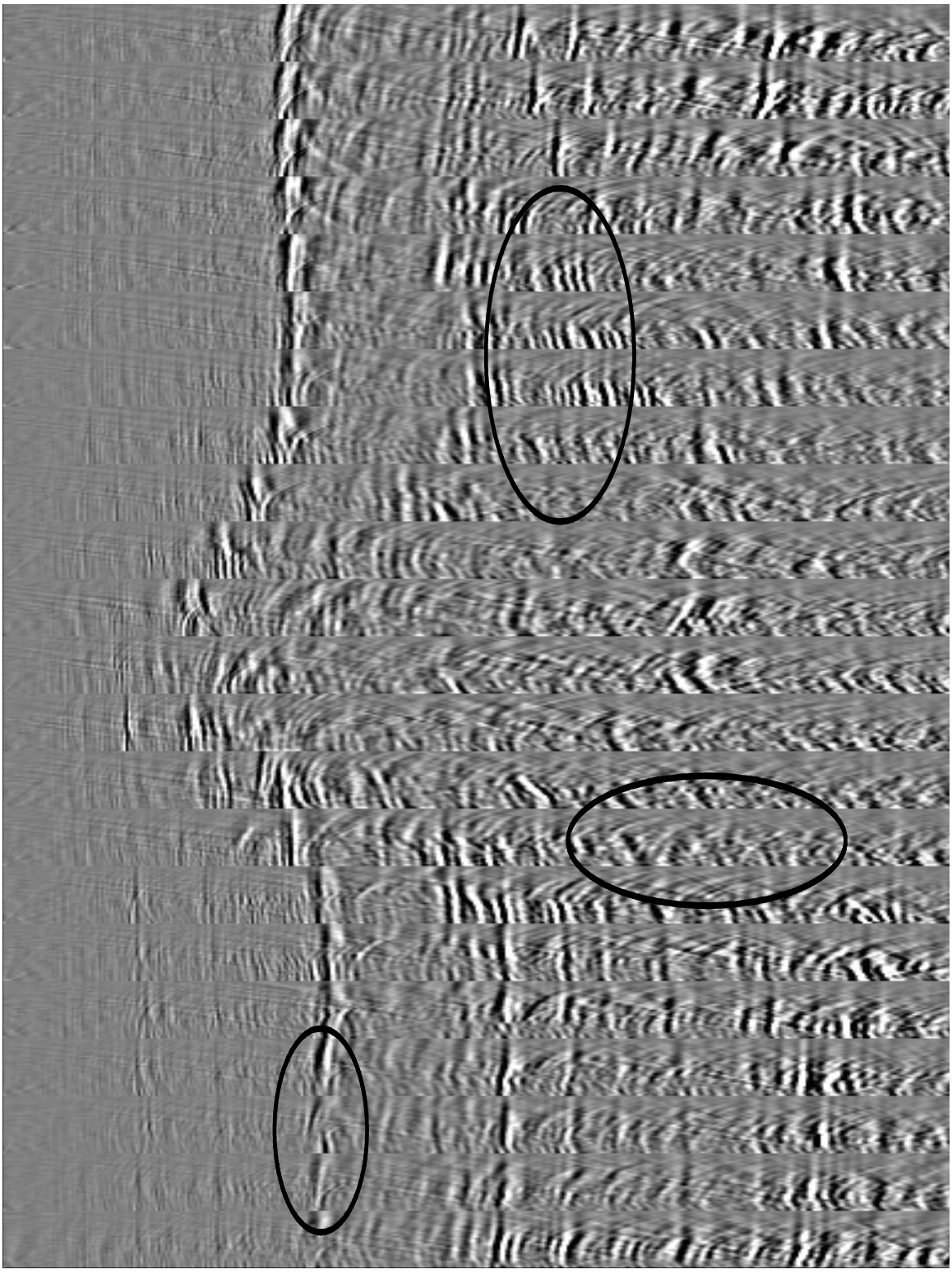

Figure 1.4: Every 20th CRP gather from the initial migration. The circled areas show either focusing or or moveout problems. 2d-moveout-vel0 [CR]

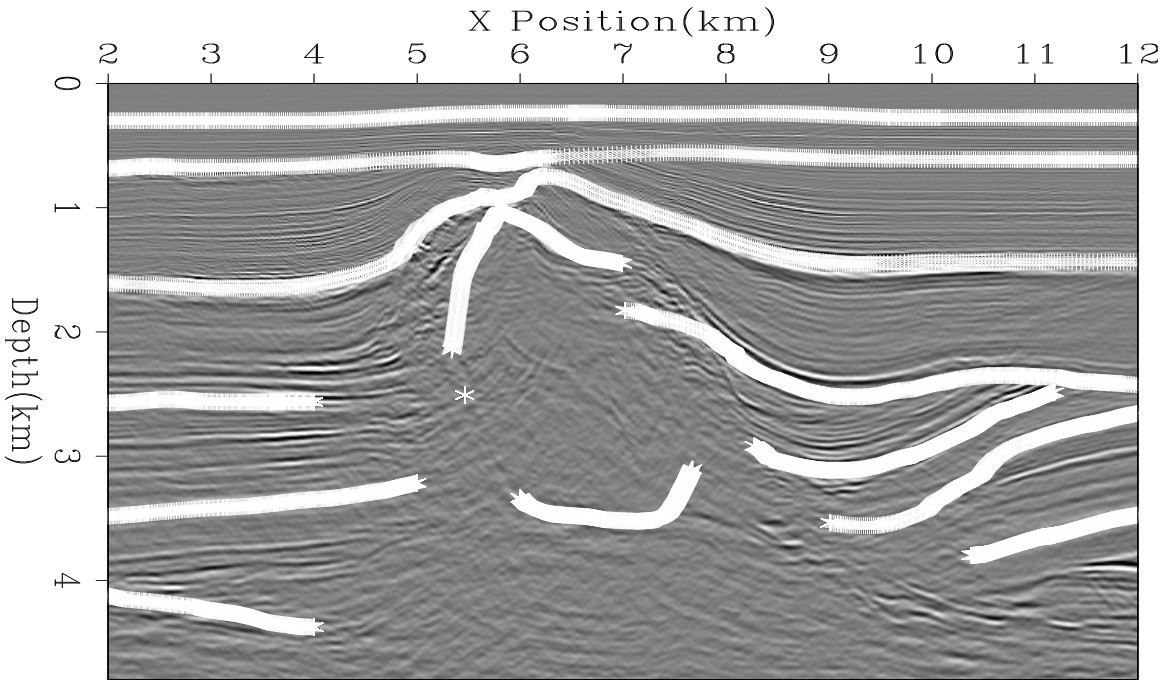

Figure 1.5: Initial migration with picked reflectors overlaid. 2d-overlays [CR]

model space. Figure 1.7 shows the interpolated dip field and the result of applying $\frac{1}{\mathbf{A}\mathbf{A}'}$ to random noise. As you can see the preconditioning operator tends to create low frequency changes fairly flat in the left portion of the model and more "U" shaped changes to the right of the salt.

The salt and salt boundary added additional complications. The sediment velocity abutting the salt dome is significantly different from the salt velocity. Using fitting goals (**??**) would create a smooth transition from the sediment layers to the salt velocity instead of the sharp contrast that often occurs when salt intrudes into sediments of significantly lower velocity. As a result it was necessary to make a slight modification to the tomography fitting goals.

I introduced a new diagonal operator **V**, which is large where we want model smoothness and becomes smaller as we approach the salt boundary. Adding this operator to the model styling goal and then applying the same preconditioning trick we end up with

$$\Delta \mathbf{t} \quad \approx \quad \left(\mathbf{T}_{\tau,\mathbf{ref}} - \mathbf{T}_{\tau,\mathbf{ray}}\right) \mathbf{A}^{-1} \mathbf{V}^{-1} \mathbf{p}$$

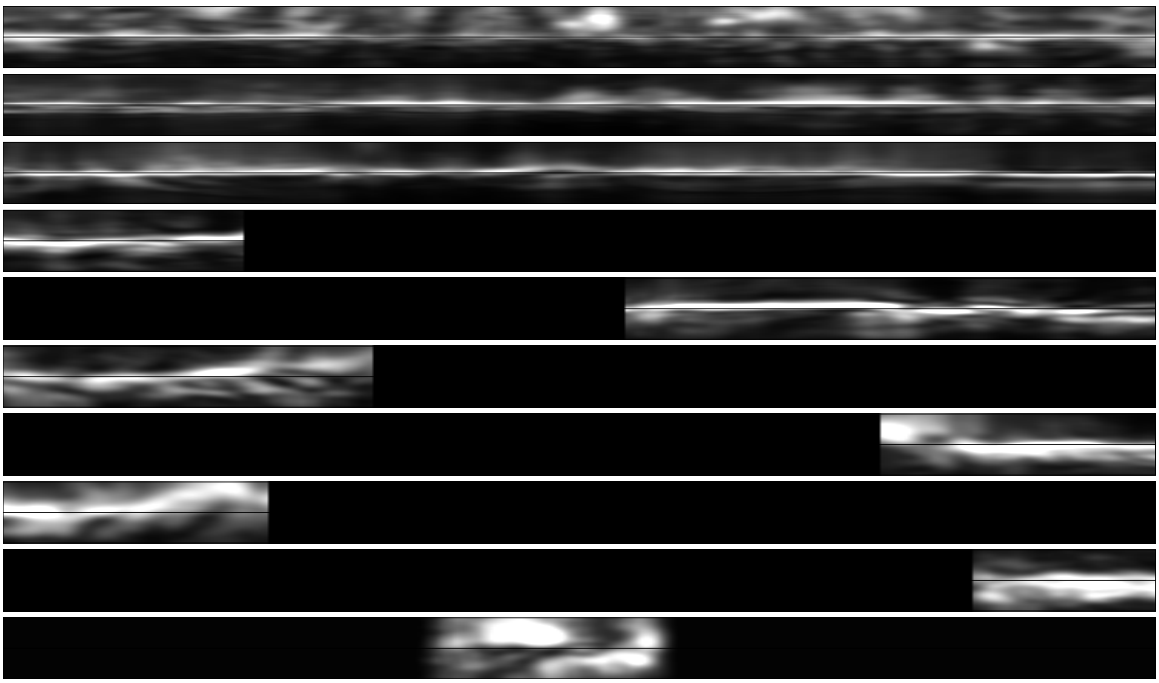

Figure 1.6: Semblance panels from ten of the reflectors used in the tomography. Note that that the top two reflectors are generally flat. The third reflector shows minimal moveout and the remaining reflectors still have significant residual moveout. 2d-elf-sem-ref.vel0 [CR,M]

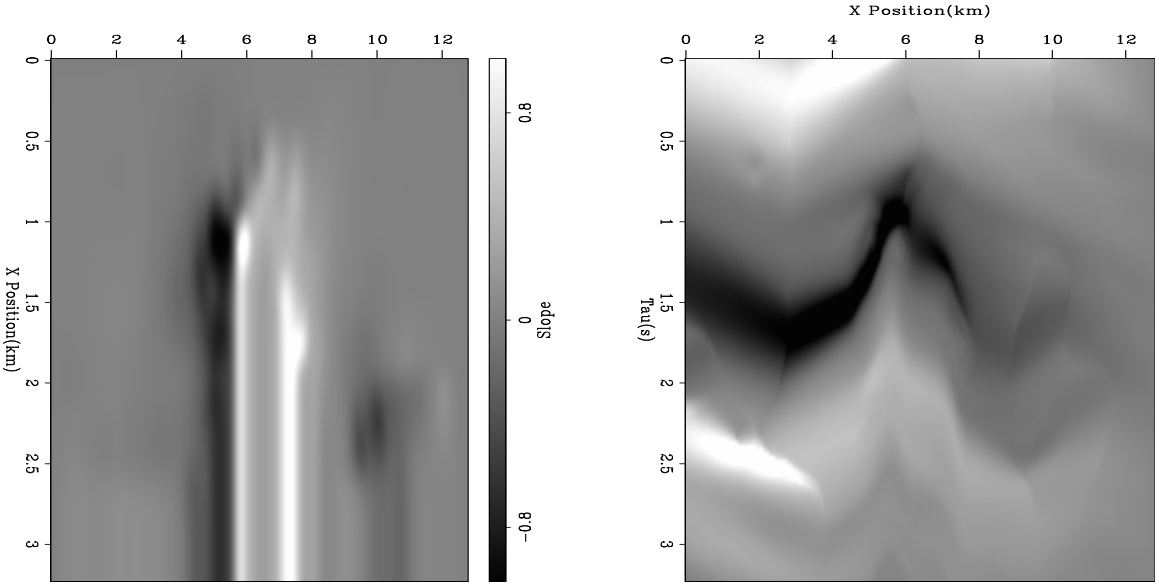

Figure 1.7: The left panel is the dip field used for the first iteration of tomography. The right panel shows the result of applying $\frac{1}{\mathbf{AA}'}$ to random noise. 2d-amp-vel0 [ER,M]

$$-\epsilon \mathbf{A}\mathbf{s_0} \quad \approx \quad \epsilon \mathbf{I}\mathbf{p}. \tag{1.1}$$

The salt itself was an additional complication. Normally salt velocity is fairly constant. Reflector continuity disappears (and therefore can not be used reliably by the tomography operator) as we get close to the salt boundary and in lower portions of the model. Very few of the raypaths used in tomography pass through the salt structure. As a result the model fitting goal would be dominated by the model styling goal and instead of a constant velocity function we would get unrealistic smooth variation in the salt velocity. To counter this problem, I followed the common practice of not allowing the salt velocity to vary.

FIRST ITERATION

Using fitting goals (1.1) I estimated a new velocity model. Figure 1.8 shows the slowness perturbations introduced to the model. Note how the changes generally follow structure. If we add these slowness changes to the initial slowness model and convert back into depth we get Figure 1.9. Our updated velocity model is smoother than the initial model (Figure 1.2). The chalk layer velocity has been increased and the sediment velocity along the lower left flank of the salt has been increased.

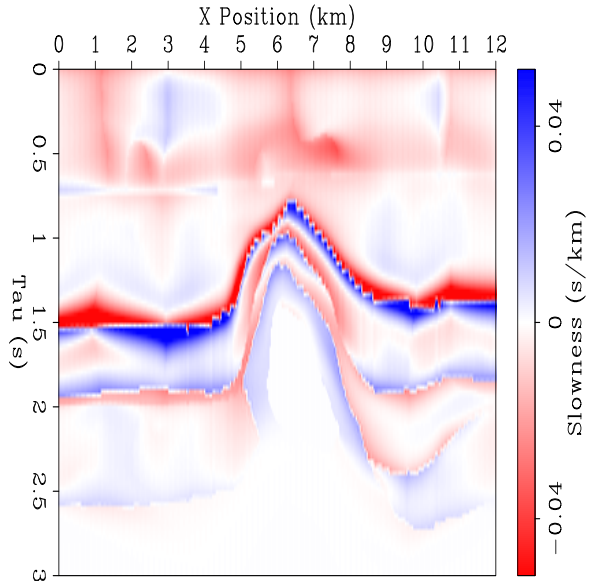

Figure 1.8: Change in slowness introduced in iteration one. 2d-change1 [CR]

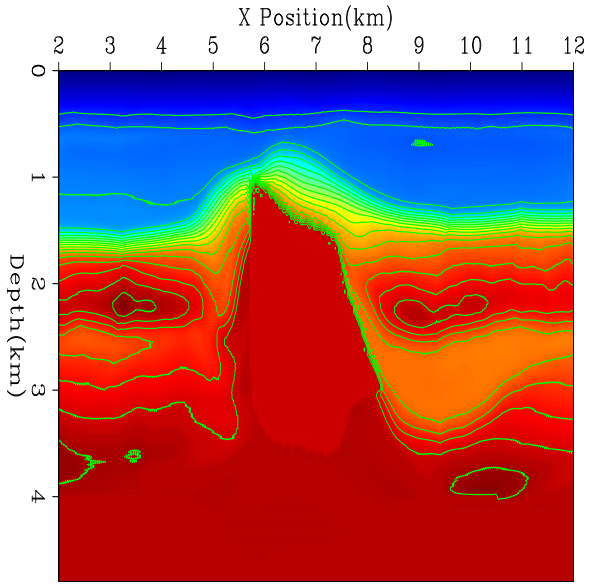

Figure 1.9: Velocity model after first iteration. 2d-vel1 [CR,M]

If we migrate using the updated velocity model, we obtain Figure 1.10. Overall the migrated image is improved. Comparing the new migration (Figure 1.10) to the initial migration result (Figure 1.3) we see that the chalk (‘D’) and salt top reflections (‘B’) are sharper. The sediments in the upper left portion of the salt flank are more coherent. We are beginning to see reflections along the lower left flank where few coherent events were present in the initial image (‘A’). The right side of the salt shows similar improvement. The focusing of the upper events is improved and we are seeing significantly more of the sediment-salt contact than was possible in the initial migration. The lower portion of the image has also improved. The salt bottom reflection is more coherent (‘C’) and we are seeing a greater extent of the reflector in the lower left portion of the image.

The CRP gathers (Figure 1.11) tell a similar story. The CRPs are flatter, and much more believable. The moveout errors have been decreased and we are now able to see more coherent events than were initially possible.

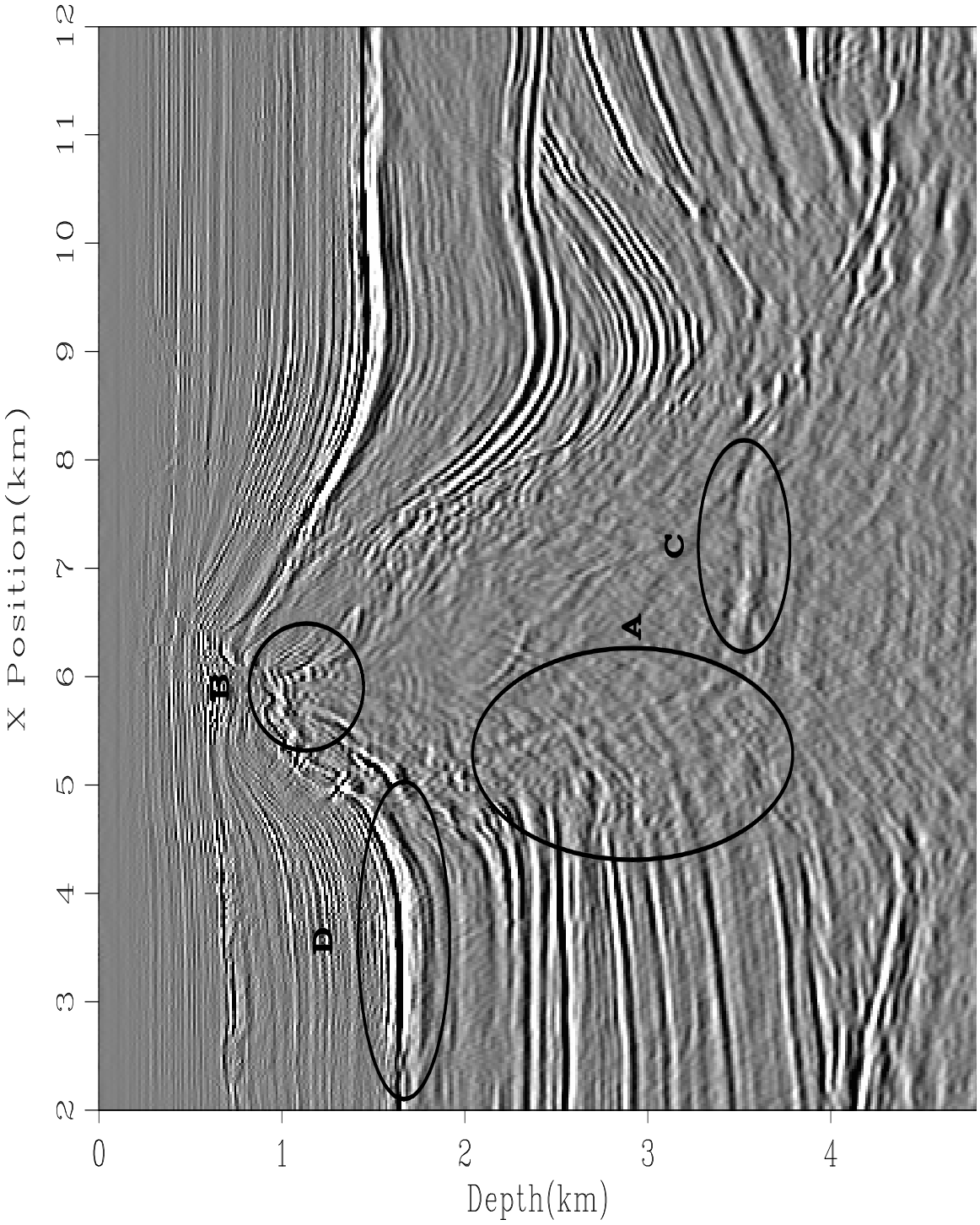

Figure 1.10: Migration result using the velocity from Figure 1.9. Locations A-D show improvement compared to Figure 1.3. 2d-elf-mig1 [CR,M]

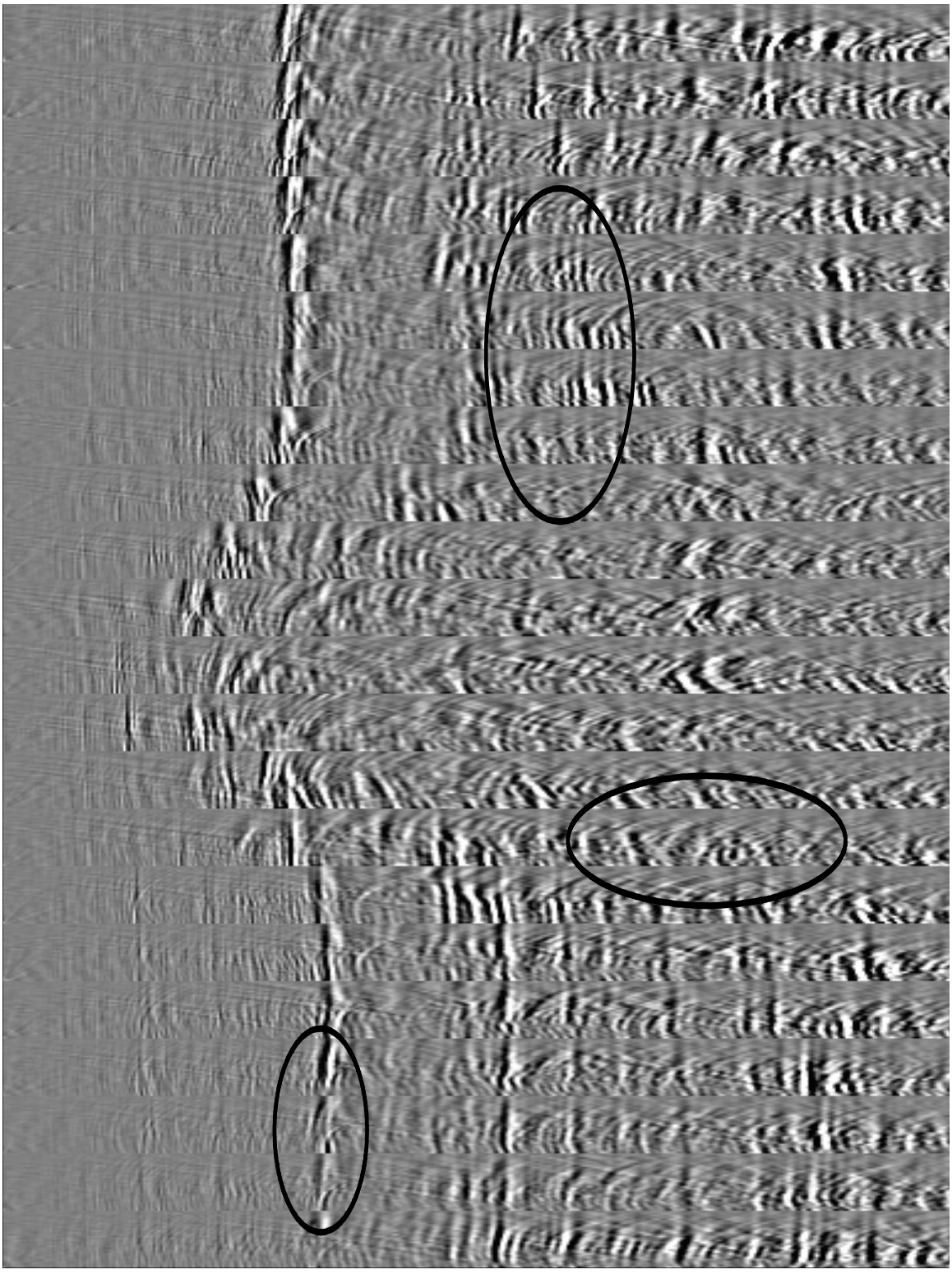

Figure 1.11: CRP gathers from the velocity after first iteration. Note how the semblance is flatter and more coherent than in the initial semblance analysis (Figure 1.4) 2d-moveout-vel1.steer [CR,M]

FINAL RESULT

If we perform another iteration of tomography we see further improvement. Figure 1.12 shows the velocity model. The velocity has been further increased in the the chalk layer on both sides of the salt ('A' and 'B'). On the right side we also see a break in the high velocity zone developing ('C'). In the Liassic where the chalk velocity was increased in the first iteration it has been decreased by the second iteration, especially on the right side of the salt dome ('D'). This decrease continues all the way to the salt edge.

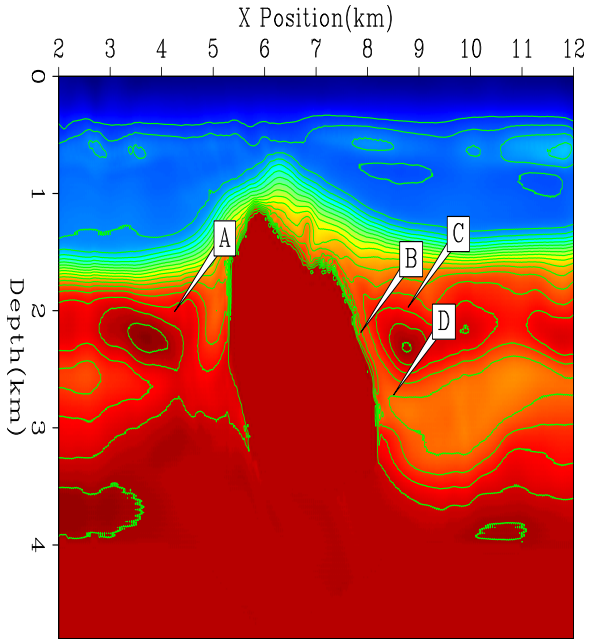

Figure 1.12: Final velocity. The velocity has been further increased in the chalk layer on both sides of the salt ('A' and 'B'). On the right side we also see a break in the high velocity zone developing ('C'). In the Liassic where the chalk velocity was increased in the first iteration it has been decreased by the second iteration, especially on the right side of the salt dome ('D'). This decrease continues all the way to the salt edge. 2d-vel-final [CR,M]

The CRP gathers (Figure 1.14) are generally flatter and more coherent. The semblance along the reflectors (Figure 1.13) is more continuous and closer to zero curvature.

The migration (Figure 1.15) using the new velocity (Figure 1.12) has also improved. The chalk layer boundary ('D') is sharper. The top of salt has fewer artifacts ('B') and the bottom of salt is more continuous ('C'). The upper reflectors on the left side of the image are more continuous. The greatest improvement is seen below the salt edge ('A'). The reflectors are more continuous and of consistent amplitude. If we look at the lower portion of the image in more detail, Figure 1.16, the differences become even more obvious. The salt reflector is flatter and continuous ('A'). The reflections to the right of the salt ('C') body are of higher frequency

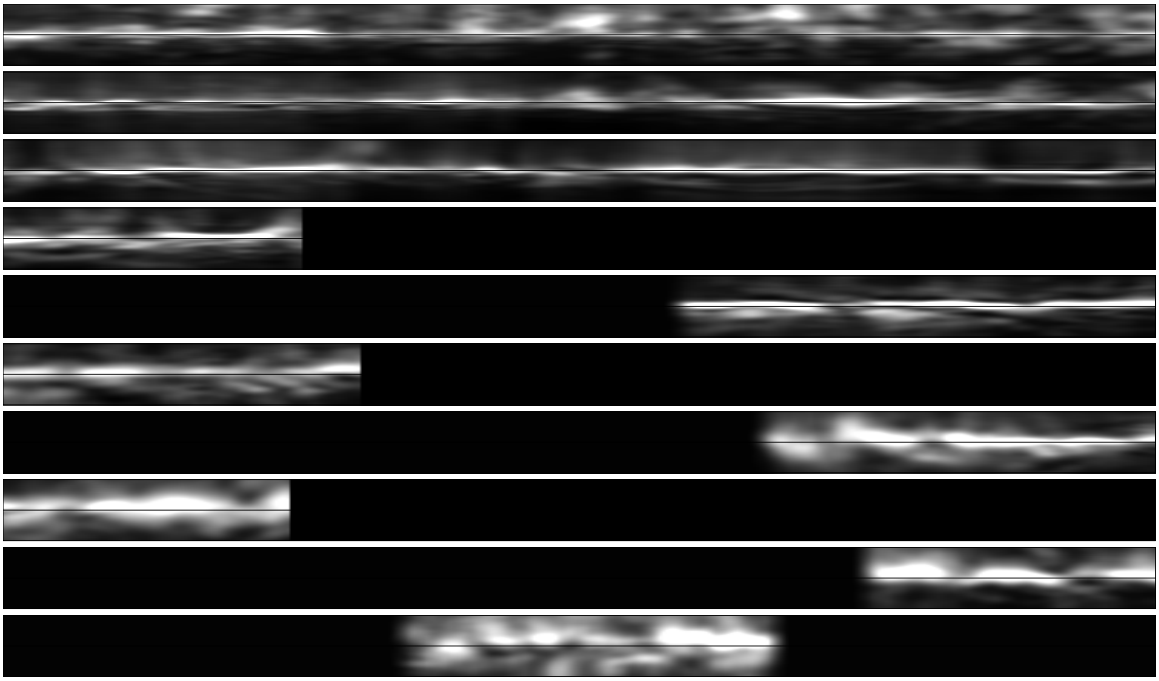

Figure 1.13: Semblance panels from ten of the reflectors used in tomography. 2d-elf-sem-ref.vel.best.steer [CR,M]

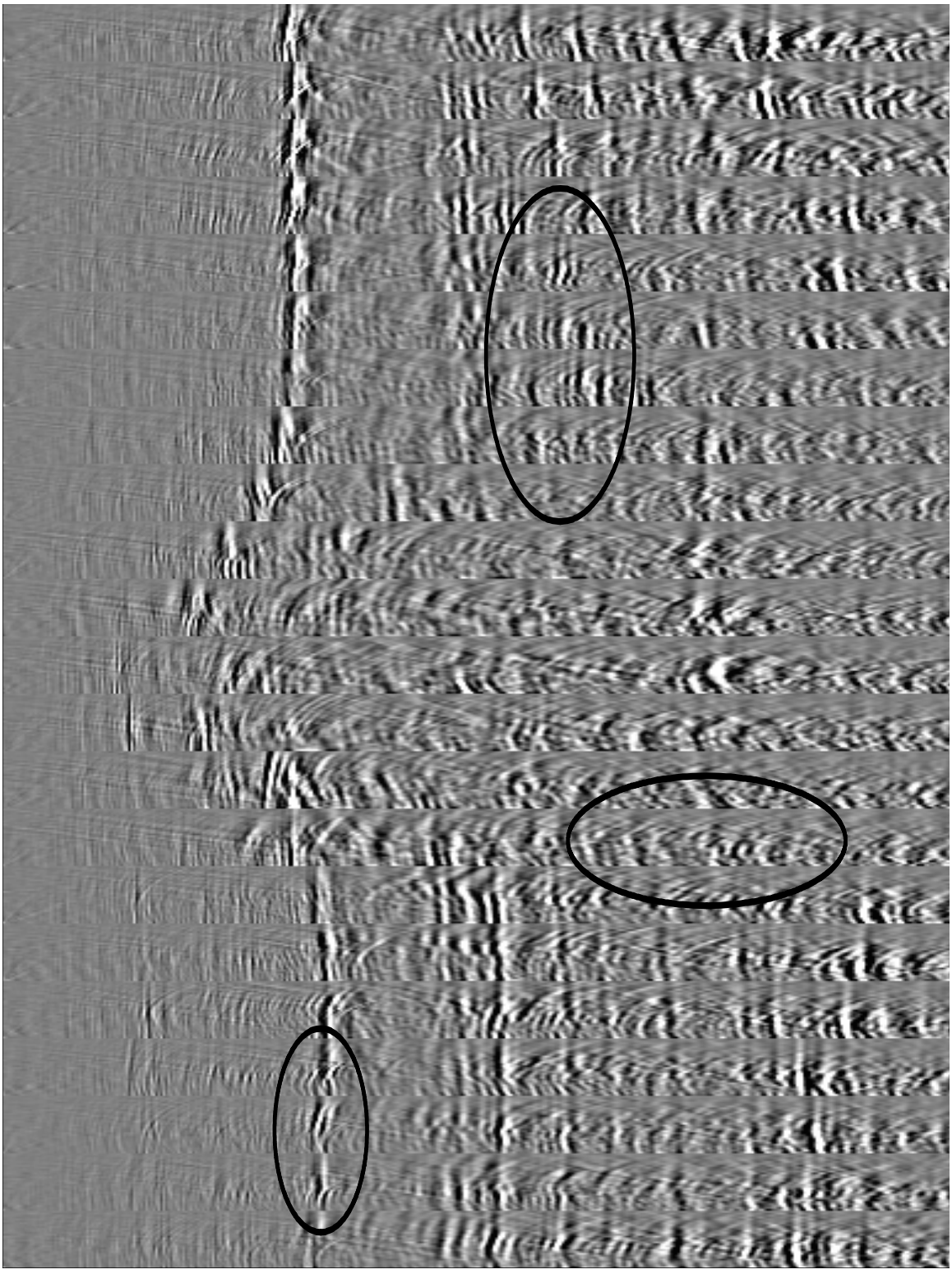

Figure 1.14: CRP gathers after the second iteration of tomography. 2d-moveout-vel.best.steer [CR,M]

and we are beginning see some structure that was not obvious in the initial migration. Below the salt edge (‘B’) we see dramatic improvement. In the initial migration, reflector continuity was lost under the salt edge. In the final migrated image we are able to continue the reflectors much further.

STARTING FROM A SMOOTH MODEL

The method presented in this thesis is an attempt to combine the best features of layer and grid based tomography. In the previous section I started from a model derived using a layer-based approach. As a result the changes were not only small amplitude (because of the good starting guess) but also relatively high frequency. In this section I take a different tack. I use the same data, but start from a vastly different velocity model (Figure 1.17). The velocity model was constructed by first drastically smoothing the initial model used in the previous section (Figure 1.2). I then migrated with this velocity, picked the salt boundaries, and added in the salt structure. Using this velocity model I then remigrated the data (Figure 1.18). The top of the salt is extremely messy and the bottom of the salt is not flat and low in amplitude. We see little below the fault at $x = 10$ km and little of the reflections below the salt edge.

A more complete test would be to start from this model and try a layer-based approach, a standard grid-based approach, and a tau-steering approach. Figure 1.2 and Figure 1.3 to some measure represent the best velocity and migrated image possible using a layer-based approach. If I do three non-linear iterations of the remaining two approaches I get the velocities in Figure 1.19. The left panel shows the result of using depth and a Laplacian smoother. Note how the velocity does not follow structure. We do not see the chalk layer bend around the top of the salt and we do not see the valley shape along the right edge of the salt. In the tau-steering approach both of these features are apparent.

Figure 1.20 shows the result migrating with each velocity. Image quality has definitely improved in both cases over the initial migrated image (Figure 1.18), but the tau-steering result is significantly better. The salt top is much cleaner in the tau-steering image than either the grid or layer based results. We are seeing more structure to the right of the salt and a better salt bottom reflection. In addition the reflectors under the salt edge are much clearer.

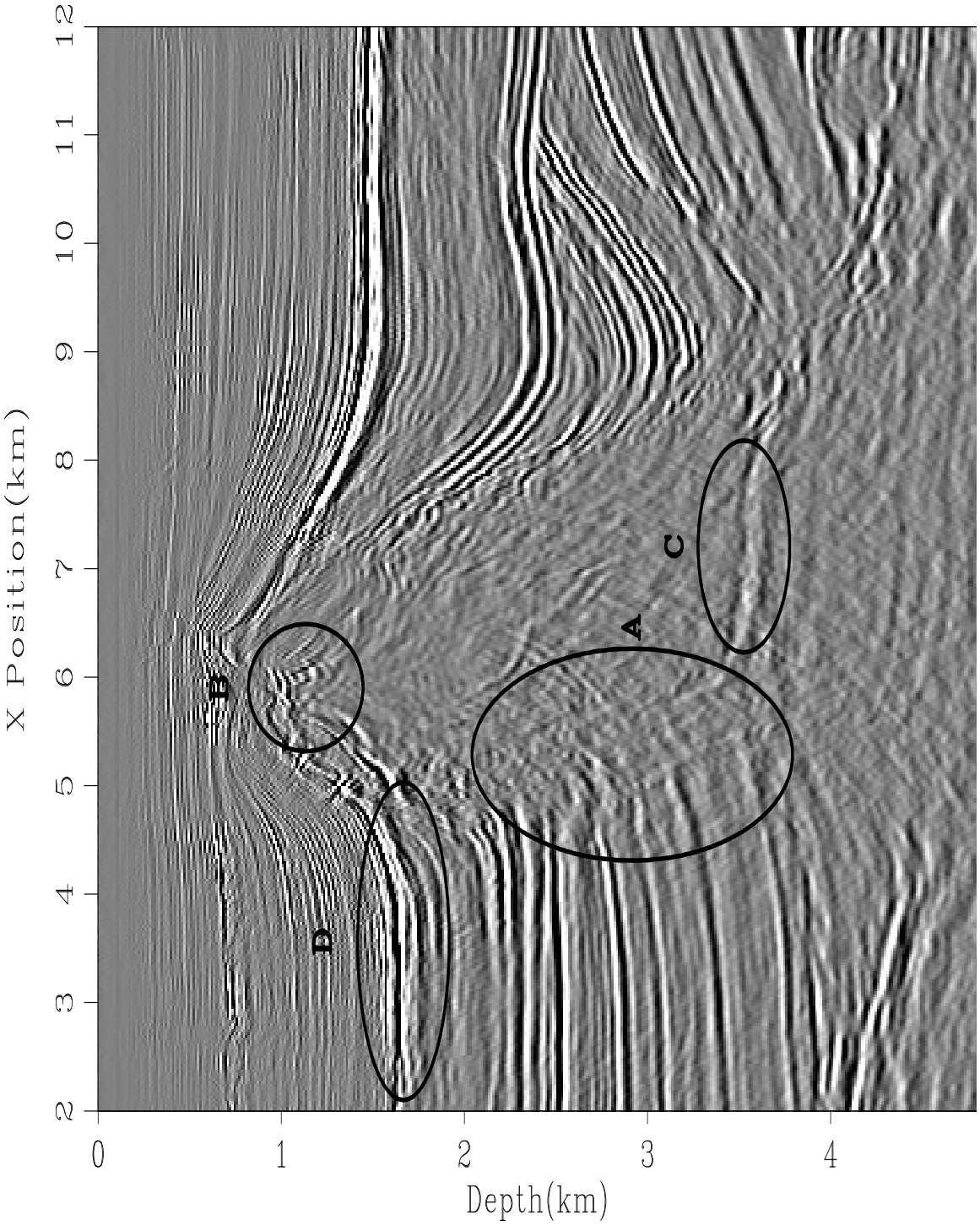

Figure 1.15: Final migrated image. Locations A-D show improvement compared to Figure 1.3. 2d-mig-final [CR,M]

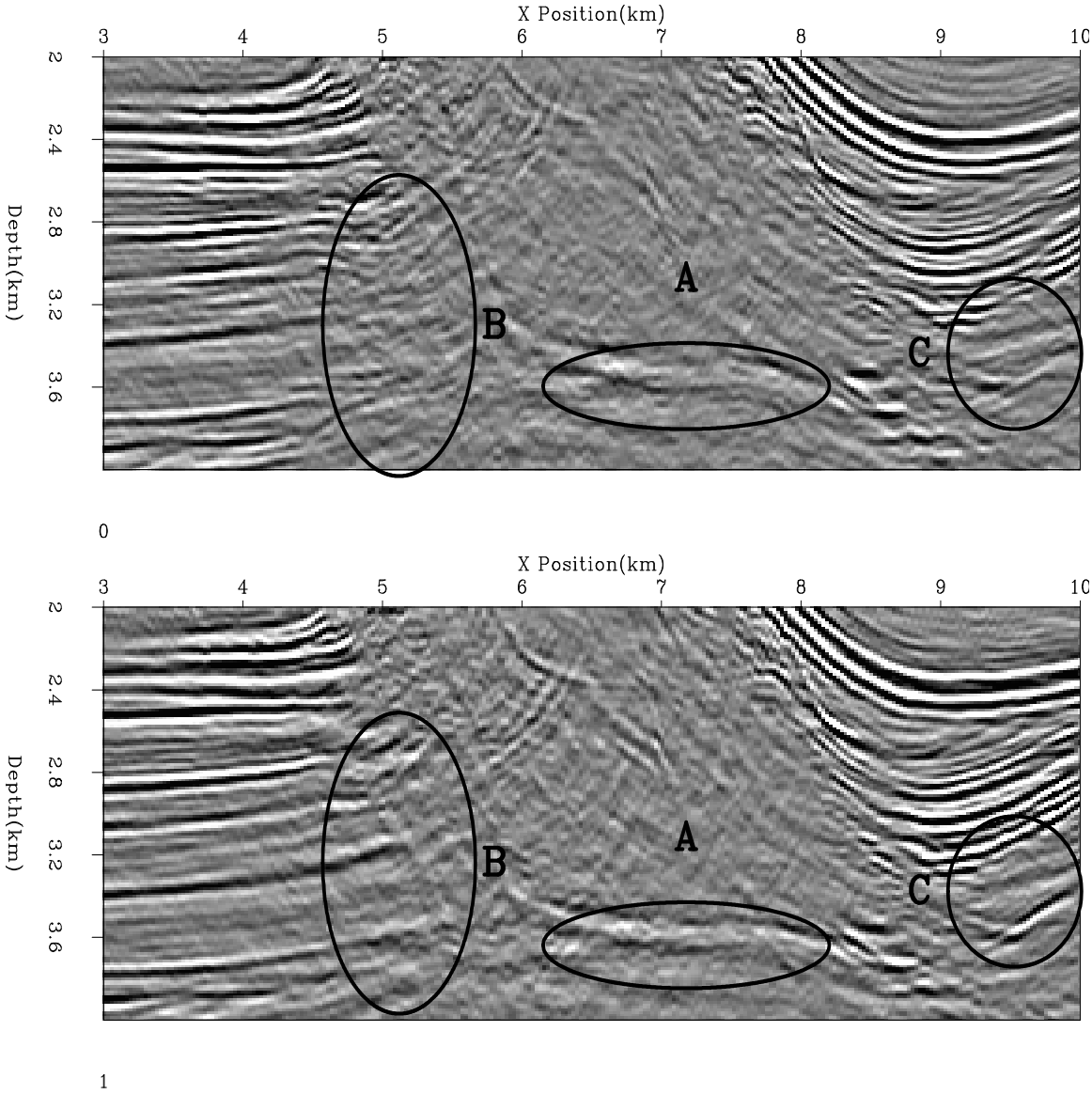

Figure 1.16: Result of migrating with the initial velocity, top panel, and the final velocity, bottom panel. We see a more coherent and believable bottom salt reflection (‘A’). The reflectors bounding the salt on the left are more continuous (‘B’) and of higher frequency (‘C’). 2d-bot.compare [CR,M]

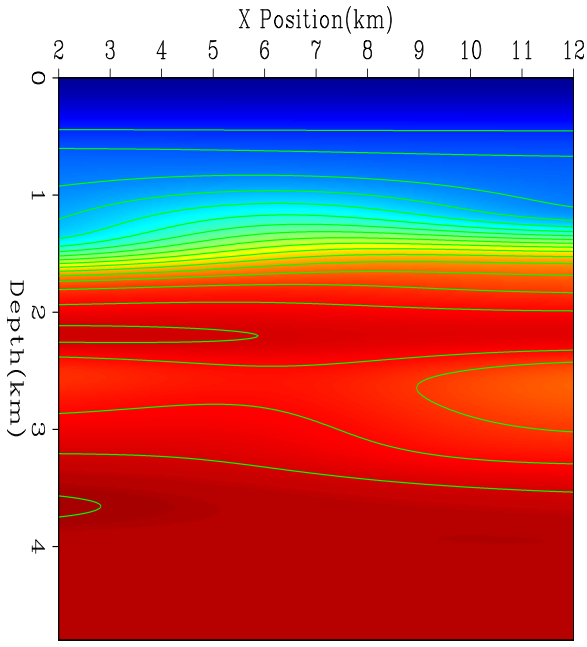

Figure 1.17: Initial smooth velocity. 2d-vel-smooth [ER]

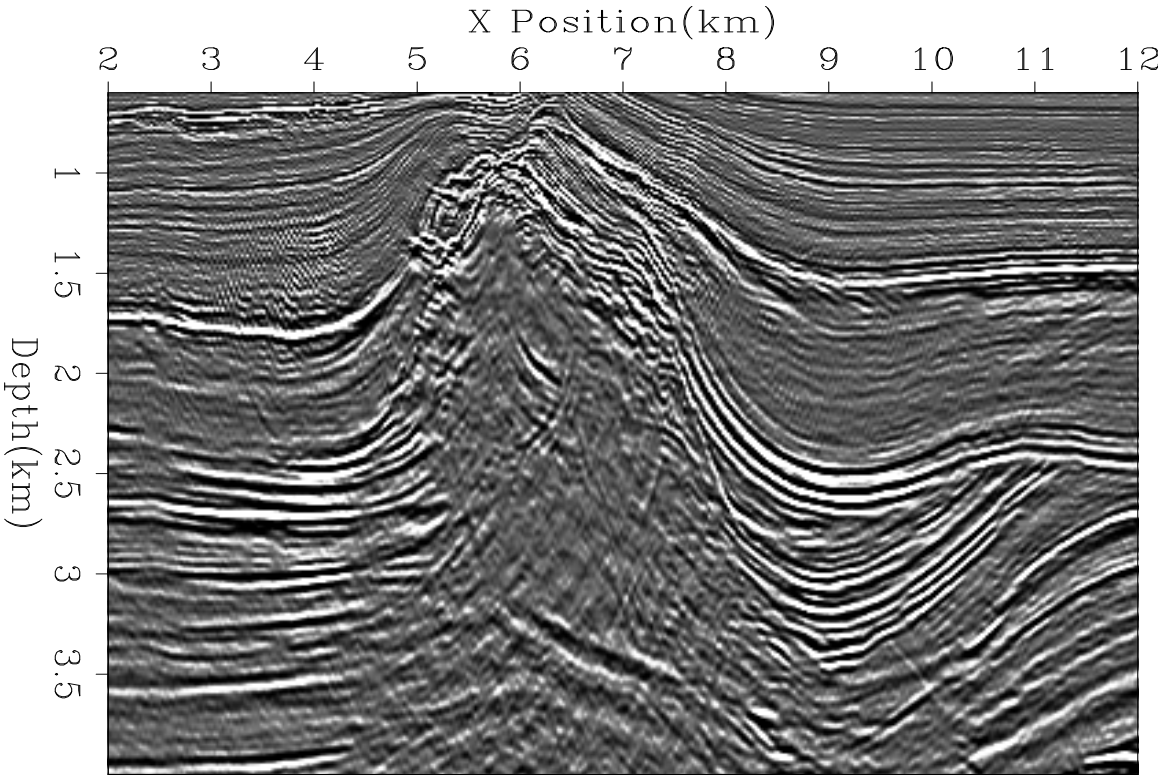

Figure 1.18: Initial migration using the velocity in Figure 1.17. 2d-elf-mig-smooth [CR]

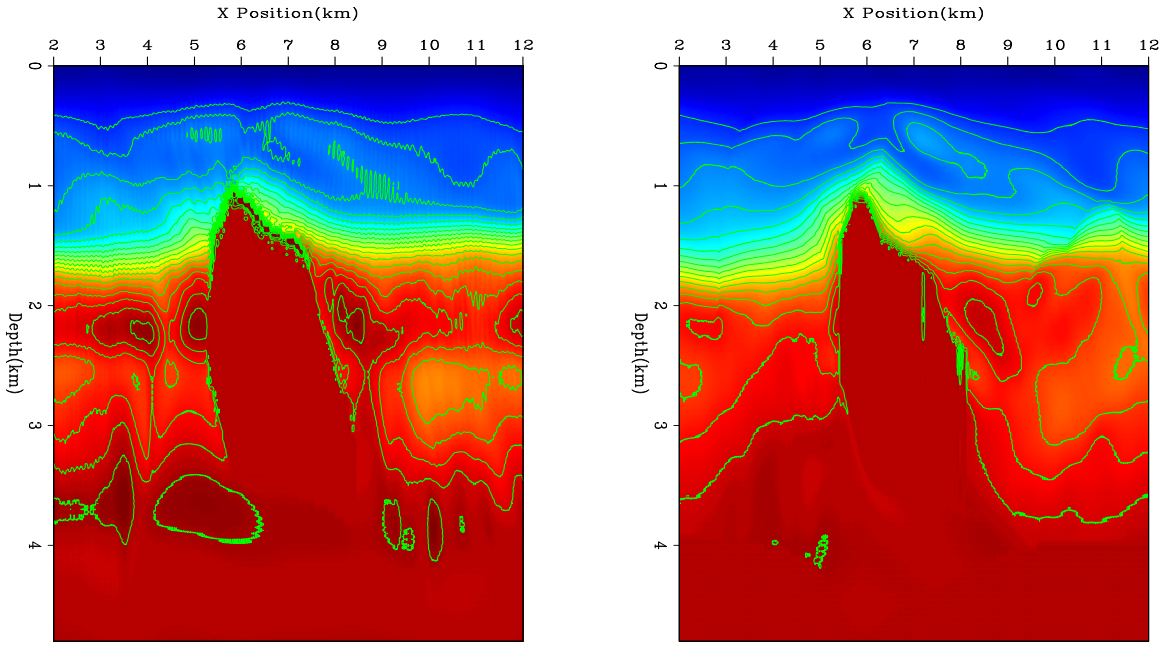

Figure 1.19: Left, depth-laplacian derived velocity. Right, tau-steering derived velocity. 2d-vel-smooth-compare [CR,M]

3-D EFFECTS

In each example presented in this chapter the final migrated image (Figures 1.15 and 1.20) still seemed to show room for improvement. The top of the salt was not well defined, especially around $x = 7$ km. We were not able to see the left salt edge and the reflectors did not extend as far as anticipated. Figure 1.21 shows some of the reason. The front panel shows the same cross-line location used in this chapter. The right panel shows a cross-line view of the structure along the upper salt top. The complicated cross-line structure means that a 2-D method has little chance of either finding the correct velocity or properly imaging. Reflectors below the salt edge are also effected by this 3-D structure. In chapter **??** I show how many of these problems are solved when the problem is addressed in a 3-D context.

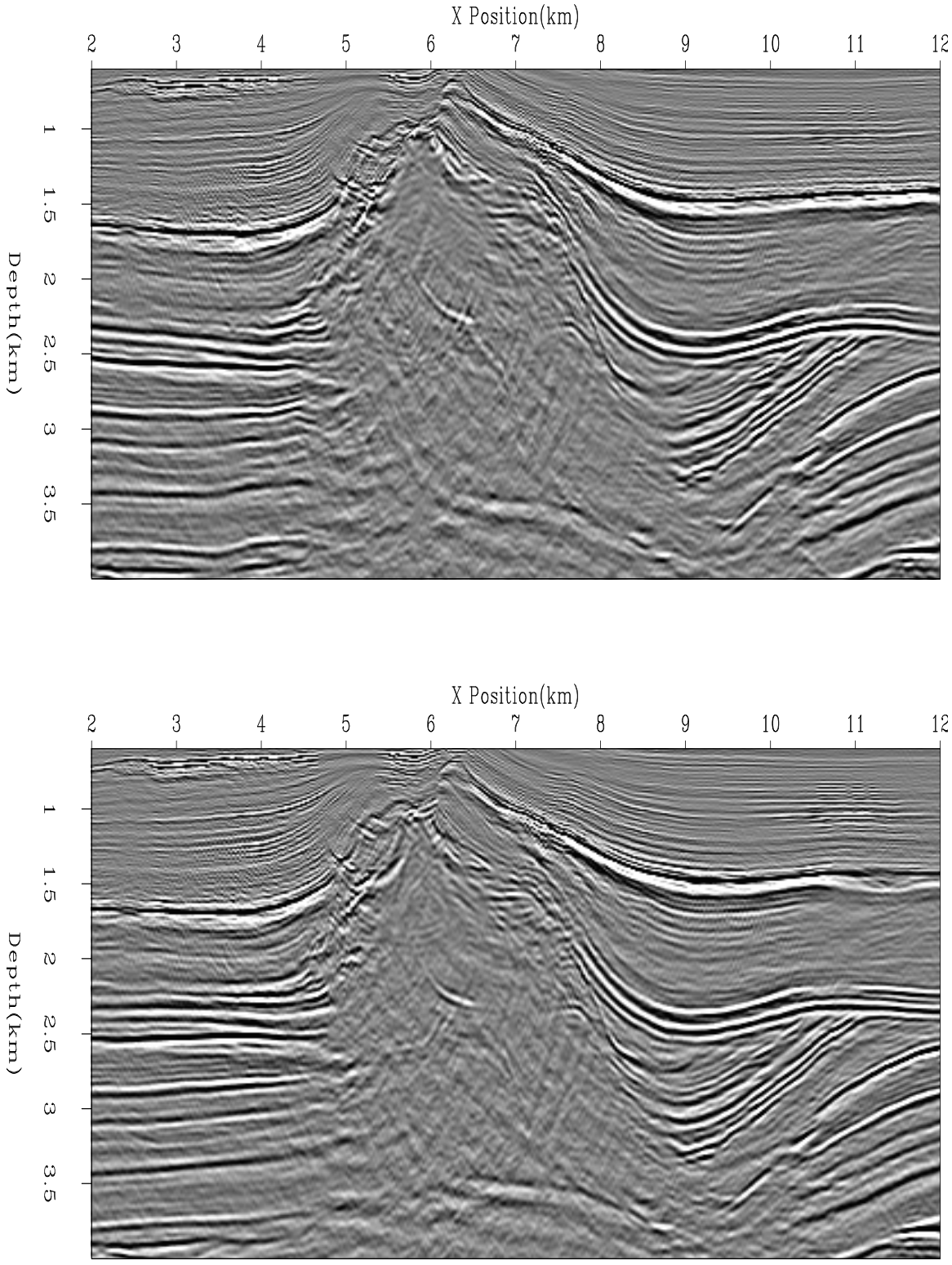

Figure 1.20: Final migration in depth-laplacian (top) and tau-steering (bottom). The velocity for each can be found in Figure 1.19. 2d-elf-mig-smooth-compare [CR,M]

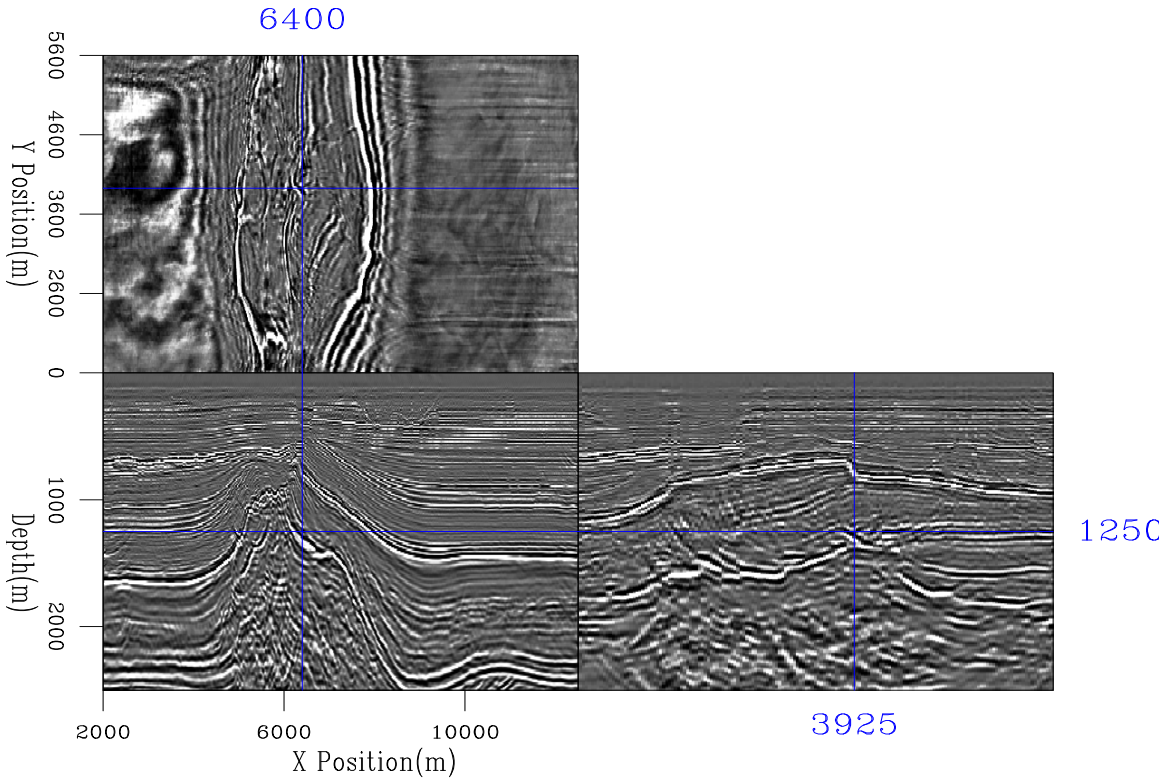

Figure 1.21: The front panel shows the same cross-line location used in this chapter. The right panel shows a cross-line view of the structure along the upper salt top. The complicated cross-line structure means that a 2-D method has little chance of either finding the correct velocity or properly imaging. 2d-3deffect [NR]

CONCLUSIONS

In this chapter I applied the tomography methodology described in Chapters **??** and **??** to 2 - D dataset. I showed how to construct a complex steering filter operator based on reflector geometry and *a priori* knowledge of the acoustic properties of the layers. The final migration result was significantly improved over the initial migration showing flatter angle gathers and overall crisper image. I hypothesize that much of the remaining moveout is due to 3-D effects, not resolvable by 2-D tomography.

Bibliography

Biondi, B., Fomel, S., and Chemingui, N., 1998, Azimuth moveout for 3-D prestack imaging: Geophysics, **63**, no. 2, 574–588.

Ehinger, A., and Lailly, P., 1995, Velocity model determination by the SMART method, part 1: Theory: 65th Annual Internat. Mtg., Soc. Expl. Geophys., Expanded Abstracts, 739–742.

Jacobs, J. A. C., Delprat-Jannaud, F., Ehinger, A., and Lailly, P., 1992, Sequential migration-aided reflection tomography: A tool for imaging complex structures: 62nd Annual Internat. Mtg., Soc. Expl. Geophys., Expanded Abstracts, 1054–1057.

Malcotti, H., and Biondi, B., 1998, Accurate linear interpolation in the extended split-step migration: SEP–**97**, 61–72.

Prucha, M. L., Clapp, R. G., and Biondi, B. L., 1998, Imaging under the edges of salt bodies: Analysis of an Elf North Sea dataset: SEP–**97**, 35–44.